Stable isotopes in precipitation and meteoric water: Sourcing and tracing the North American monsoon in Arizona, New Mexico, and Utah

C.L. Tulley-Cordova[1,2], A.L. Putman[2], and G.J. Bowen[2]

[1]Navajo Nation Water Management Branch, Fort Defiance, AZ, USA.

[2]Department of Geology and Geophysics, University of Utah, Salt Lake City, UT, USA.

Corresponding author: Crystal Tulley-Cordova (tulleycordova@gmail.com)

Key Points:

1. A prominent seasonal maximum in Four Corners-region precipitation isotope ratios occurs during the peak of the North American Monsoon
2. Peak monsoon precipitation isotope ratios are similar across broad geographic regions, reflecting intensive land-surface recycling
3. Monsoon water contributes minimally to runoff and groundwater recharge, its primary fate is evapotranspiration

Abstract

The North American monsoon (NAM) is an important source of precipitation across the southwestern United States (US). The approximate northern boundary of this feature crosses the Navajo Nation, in the Four Corners region, where NAM rains have long been important to the livelihoods of Native Americans. Relatively little is known about the characteristics and hydrological significance of the NAM in this region. Here we report a new 4-year record of stable H and O isotope ratios in monsoon-season rainfall and water resources across the Navajo Nation. Monthly precipitation samples collected at 39 sites document a characteristic pattern of ^{2}H- and ^{18}O-enrichment associated with monsoonal precipitation. These changes are weakly correlated with local precipitation intensity, however, and the correlation that does exist is dominated by sub-cloud evaporation effects. In contrast to precipitation amount, monsoon-season isotopic values exhibited limited spatial variability across the region, and after correction for sub-cloud evaporation Navajo Nation values were similar to those from a site in southern Arizona. Airmass back-trajectory analysis suggests that the uniformly high NAM isotope values across the region may reflect 1) a region-wide shift from mid-latitude to low-latitude moisture sources at the onset of the peak monsoon, and 2) substantial land-surface recycling of NAM moisture in upwind regions. Comparison of precipitation isotope data with surface and groundwater values implies that, despite its hydroclimatic significance, monsoon rainfall contributes little to rand subsurface water resources. This highlights the monsoon's importance for warm-season land-surface ecology and hydrology critical to residents of the Four Corners region.

Keywords

North American Monsoon, stable isotopes, Navajo Nation, water resources, climate change

1 Introduction

Past variability in precipitation across the arid southwestern United States has been documented over a range of time scales (Carleton et al., 1990; Gutzler, 2000; Ciancarelli et al., 2014; Carrillo et al., 2016), and both wet and dry extremes have been associated with environmental and societal impacts (Adams & Comrie, 1997). Seasonal precipitation within this region is bimodal, with a pronounced summer peak associated with winter synoptic systems originating from the North Pacific and a summer maximum reflecting the North American Monsoon (Carleton et al., 1990; Schmitz & Mullen, 1996; Adams & Comrie, 1997; Hu & Dominguez, 2015; Szejner et al., 2016; Tulley−Cordova et al., 2018). Although engineered water management systems across much of this region are designed to capture and store out-of-season water, and to ameliorate risks of extreme monsoon events, vast areas of rural land remain dependent on natural water resources and exposed to risk associated with their variability. Moreover, historic data and models suggest that increases in temperature-driven evaporation and changes in precipitation amounts and patterns have and will continue to reduce water availability in this region (Seager et al., 2007; Redsteer et al., 2010), and together with the potential for severe drought events (Cook et al., 2004) threaten sustainability of existing water infrastructure (Overpeck & Udall, 2010; Milly & Dunne, 2020).

The Diné Bikeyah, also known as the Navajo Nation ("NN"), spanning the "Four Corners" region of the current states of Utah, Colorado, New Mexico and Arizona, is the largest land-based Native American tribe in the United States, with an area over 70,000 square kilometers (Novak, 2007; Nania et al., 2014; Guiterman, 2015). Like many Indigenous peoples, the Navajo are particularly vulnerable to the impacts of climate change due to the arid environmental

65 conditions across their homelands and their traditional ways of life (Redsteer et al., 2013;
66 Wildcat, 2013; Nania et al., 2014; Bennett et al., 2017). The NN sits nearly the northern
67 boundary of the modern NAM region. Annual average precipitation ranges from 67 mm in low-
68 lying, northern areas to 738 mm in some high elevation areas (Tulley−Cordova et al., 2018). All
69 areas of the NN experience a pronounced peak in precipitation during the summer associated
70 with the NAM. This peak represents ~60%, on average, of annual precipitation in low-elevation
71 areas and ~40% in in the mountains, but with substantial inter-annual variability (~20 to 80%) at
72 all elevations (Tulley−Cordova et al., 2018). In most years, summer monsoon rains in the Four
73 Corners region begin in July and extent through September, with peak rainfall occurring in July
74 in the far eastern part of the region and August elsewhere.
75
76 Previous research has investigated the dynamics and history of the NAM across the broader
77 southwestern USA. Modeling studies have highlighted two branches of the NAM, stemming
78 from Gulf of California (GoC) and Gulf of Mexico (GoM), and associated their contributions to
79 NAM rainfall with the depth and position of the low pressure system over the southwest
80 (Carleton et al., 1990; Schmitz & Mullen, 1996; Adams & Comrie, 1997). Recycling of water
81 from the land surface (through evaporation and transpiration) is thought to be a major source of
82 moisture to monsoon precipitation across parts of the NAM region (Bosilovich, 2003; Hu &
83 Dominguez, 2015). Hu & Dominguez (2015) also demonstrated a distinction between the
84 isotopic composition of monsoon moisture derived from GoM (higher values) and Pacific/GoC
85 sources (lower), suggesting that isotopes may be useful in reconstructing moisture transport
86 patterns across the NAM region. Although their analysis did not clearly distinguish isotope
87 values characteristic of recycled moisture, these authors present evidence that recycled moisture,

88 which is accompanied by limited isotopic change (Ingraham & Taylor, 1991; Chamberlain et al.,
89 2014), may preserve isotopic differences associated with different marine sources. Isotopic
90 contrasts between NAM and winter precipitation in this region may also provide a basis for
91 quantifying seasonal sources of water used by plants (Williams & Ehleringer, 2000) and, through
92 isotopic measurements of proxies such as plant-derived biomarkers, reconstructing past variation
93 in monsoon strength (Bhattacharya et al., 2018).
94
95 Despite our growing understanding of the NAM and its variability, projecting and planning for
96 impacts of future NAM change requires additional work that further characterizes this feature of
97 the hydroclimate and its impacts at local to regional scales relevant to management and policy. In
98 this study we report and interpret a new 4-year monitoring record of precipitation and water
99 resource H and O isotope values at sites across the NN. We characterize spatial and temporal
100 isotopic patterns associated with NAM precipitation, evaluate the climatic processes that drive
101 these patterns, and assess the contribution of NAM rainfall to water resources in this region. In
102 addition to their relevance for understanding the modern NAM and its hydrological significance,
103 these results should help inform future reconstructions of past NAM change based on isotopic
104 proxy data.

105 **2 Methods**

106 2.1 Precipitation Monitoring

107 The precipitation gauge on the NN was installed in 1952. Since that time, the Navajo Nation
108 Water Management Branch's Water Monitoring and Inventory Group (NNWMB) has managed
109 over 190 precipitation gauges, as well as multiple snow survey and stream gaging sites, within
110 their hydrometeorological network (Garfin et al., 2007; Aggett et al., 2011; Hart & Fisk, 2014;

111 Tsinnajinnie et al., 2018; Tulley−Cordova et al., 2018). The precipitation data from the
112 NNWMB network documents regional hydroclimate across this large, remote region at a spatial
113 extent and coverage not available from other methods (e.g., satellite and radar; Crimmins et al.,
114 2013). Given the limited telecommunication and electrical infrastructure of the Four Corners
115 region, data from most stations reflect total accumulations within rain cans, recorded manually at
116 monthly intervals (Aggett et al., 2011; Tulley−Cordova et al., 2018).
117

118 2.2 Precipitation Sampling

119 We selected 39 sites from the NNWMB's hydrometeorological network for monthly
120 precipitation collection and isotopic analysis (Figure 1). Samples were collected from May to
121 October, 2014 to 2017. At two of the 39 sites (Fort Defiance, AZ and Rock Springs, NM),
122 additional event-scale sampling was performed from May to October, 2015 to 2017. For the
123 Rock Springs site, event-based sampling was extended through the winter months during 2016
124 and 2017 to produce a full-year record. A total of 1,084 precipitation samples were collected, and
125 data were grouped for analysis into samples representing pre-monsoon (April – June), monsoon
126 (July – September), and post-monsoon (including winter; October – March) seasons.
127

128 Precipitation was collected in custom-built devices consisting of a 10.2 cm diameter funnel
129 connected to a 1 L, narrow mouth, Nalgene HDPE bottle using vinyl tubing and brass barb
130 fittings. Silicone adhesive was used to secure and seal parts, and the collection tubing was
131 extended to the bottom of the collection bottle to ensure that the bottom end was submerged after
132 a small volume of precipitation had been collected. A small (2 mm) vent hole was drilled in the
133 cap of the sample bottle to allow air from the bottle to escape as water entered. The collector was

placed in a 66.0 cm long holder made from polyvinyl chloride (PVC) pipe, the bottom of which was buried and anchored in the ground. Following the 2014 collection season, several mL of mineral oil was added to each collector to prevent evaporation (2014 collections did not use oil, see discussion in the Results section).

Samples were collected at monthly intervals (monthly samples) or as soon as possible after precipitation events (event samples) and were weighed to determine the total precipitation amount (subtracting the combined weight of the bottle and mineral oil). We obtained an 8 mL aliquot of water (if available) from the bottle using a syringe, which was transferred to a glass rubber-seal sample bottle for storage. Samples from oil-containing collectors were filtered through a 0.45 um nylon syringe filter prior to storage. After sample collection, the collector bottle was replaced with a cleaned, dry bottle.

2.3 Water Resource Collection

We sampled a range of groundwater, lakes, and streams across the study area for stable isotopic analysis. All samples were collected in 4 mL glass vials with rubber lined closures, immediately capped, and the closure secured with Parafilm®. Groundwater samples (672) were gathered from 185 groundwater wells (Figure 1) in collaboration with Navajo Tribal Utility Authority (NTUA) drinking water compliance sampling conducted between March and September each year from 2014 to 2017. Lake samples were obtained from natural lakes and reservoirs by dip-sampling from the lake shore. Springs were sampled as close as possible to the point of discharge, either directly from a seep or from spring pools. Dip samples of ephemeral and perennial streams were collected from actively flowing parts of the stream. Each of these types of surface-collected

157 samples were collected intermittently during the calendar year from 2014 to 2017. Overall, 58
158 lake, 116 stream, and 46 spring samples were obtained at 7, 25, and 45 sites, respectively (Figure
159 1).
160
161 2.4 Isotope Analysis
162 Samples were stored in a refrigerator at 4°C prior to analysis. Stable H and O isotope ratios were
163 analyzed at the University of Utah Stable Isotope Ratios for Environmental Research (SIRFER)
164 facility using a Cavity Ring-Down Spectroscopy instrument (Picarro L2130-i). All samples were
165 calibrated to the Vienna Standard Mean Ocean Water (VSMOW) Standard Light Antarctic
166 Precipitation (SLAP) reference scale based on data from co-analyzed reference waters (PZ:
167 16.9‰, 1.65‰; PT: −45.6‰, −7.23‰; UT: −123.1‰, −16.52‰; for δ^2H and $\delta^{18}O$, respectively).
168 Sample values are reported in δ notation, where $\delta = R_{sample}/R_{standard} - 1$ and $R = {}^2H/{}^1H$ or ${}^{18}O/{}^{16}O$.
169 Sample values represent an average of four replicate injections, with corrections applied for
170 through-run drift and memory effects (Good et al., 2014).
171
172 To complement the NN data, we use published monthly-average precipitation isotope data
173 collected in Tucson, Arizona (Eastoe & Dettman, 2016), which were accessed from the
174 University of Arizona Environmental Isotope Laboratory Data Repository
175 (https://www.geo.arizona.edu/node/154, accessed 12/18/2020). Values for individual months
176 were averaged (without weighting) to obtain long-term average monthly values characterizing
177 the annual cycle at Tucson.
178
179 2.5 Data Analysis

We use an updated version of the iSW_E (isotopic source water estimation with evaporation) model of Bowen et al. (2018) to assess the effect of post-condensation evaporation on precipitation samples and infer contributions of NAM and winter-season precipitation to surface and subsurface water resources. Briefly, the model predicts the measured isotopic composition (δ_{obs}) of a water sample from the values of an un-evaporated source water (δ_s) as:

$$\delta^{18}O_{obs} = \delta^{18}O_s + E, \text{ and} \quad (1)$$

$$\delta^{2}H_{obs} = \delta^{2}H_s + E \times m, \quad (2)$$

where E is an evaporation index (in units of $\delta^{18}O$ ‰) and m is the slope of an evaporation line. Prior estimates are provided for each term on the right side of the equations, and the model is inverted using Bayes Rule to obtain a posterior distribution for all model parameters conditioned on the observed sample values. A uniform distribution bounded on 0 and 15‰ is used to evaluate a wider range of possible evaporation effect sizes, and a normal prior centered on 5 for all NN data and 4.8 for Tucson rainfall ($1\sigma = 0.3$) is used for the evaporation line slope based on the regional surface-water evaporation line values estimated by Bowen et al. (2018). The value of m is somewhat uncertain, and we tested the impact of using slightly different slope estimates (e.g., 5.5 ± 0.3); this produced only minor differences from the results presented here (not shown).

Prior estimates of the source values are specified in one of two ways. For analysis of pre-evaporation compositions of precipitation samples, the prior distribution is constrained by the

203 statistics of the global meteoric water line (GMWL), representing the global mean covariant
204 relationship between precipitation δ^2H and $\delta^{18}O$ values (Bowen et al., 2018). Although local
205 deviations from this relationship can be expected due to vapor source characteristics (Putman et
206 al., 2019), we prefer to characterize precipitation source values using the GMWL rather than a
207 local meteoric water line estimated from ground-based precipitation sampling because of the
208 potentially strong influence of sub-cloud re-evaporation of hydrometeors on the latter (see
209 Results and Discussion). For analysis of surface and groundwater resources, source values are
210 modeled as a linear mixture of two seasonal endmembers, each of which is represented by a
211 bivariate normal distribution. The summer NAM endmember was approximated to reflect the
212 variability among average NAM-season (July-September) precipitation isotope values at
213 different monitoring sites (based on sampling from the observed averages with replacement); the
214 distribution values for this endmember are -42, -5.7, 8.6, 1.8, and 14.5 (δ^2H, $\delta^{18}O$, δ^2H 1σ, $\delta^{18}O$
215 1σ, and covariance, respectively). Since only a small number of winter precipitation data were
216 collected, the endmember distribution was approximated by sampling three events from the
217 individual data (November - March) with replacement and averaging; 10,000 such samples were
218 drawn to characterize a distribution reflecting integration of event values but retaining a
219 conservative (high) level of variability (parameter values: -82.9, -11.9, 14.2, 1.7, and 24.5). The
220 prior estimate on the mixing model source values, then, was parameterized in terms of these
221 endmember distributions and a NAM-source mixing fraction (f_{NAM}; winter faction = 1 - f_{NAM})
222 given by a Dirchlet distribution (shape parameters = [1,1]). We recognize that the isotopic
223 endmembers are imperfectly characterized, particularly for winter precipitation, which adds
224 potential uncertainty to the analysis. Subsequent work could address such factors as differences
225 in the elevation and age of source-water recharge that might affect mixture estimates for some of

these sample types; these factors are discussed where potentially relevant, below.

All data analysis was conducted in R version 4.0.2 (R Core Team, 2020). The functions used (*mwlSource* and *mixSource*) are available in version 0.2.1 of the *isoWater* package (Bowen, 2021), and conduct Markov Chain Monte Carlo sampling of the posterior distributions using rjags (Plummer, 2019) and R2jags (Su & Yajima, 2020). For all analyses, at least 200,000 samples were generated from each of three chains, with thinning to retain 2,500 samples per chain. Convergence was monitored using trace plots and the Gelman and Rubin convergence factor R-hat (Gelman & Rubin, 1992). We found that a burn-in period equal to 10% of the total chain length was adequate to remove any model initialization effects, and all analyses show moderate to strong convergence (R-hat < 1.03). Although the effective posterior sample size for analyses of some individual water samples was relatively small (~100), all interpretations drawn here are based on posterior samples from many (dozens if not hundreds) of water samples.

2.6 Back Trajectory Analysis

One documented control on precipitation stable isotope ratios is variation in vapor source region (Ichiyanagi & Yamanaka, 2005; Treble et al., 2005; Strong et al., 2007; Sodemann et al., 2008; Good et al., 2014; Putman, Feng, Sonder, et al., 2017). We evaluated the vapor source regions contributing to each pre-monsoon and monsoon season precipitation event sampled at Fort Defiance and Rock Springs in 2015-2017 using Lagrangian back trajectory analysis. Our analysis followed the procedure presented in Putman et al. (2017). In short, this method uses reanalysis data (https://www.ncdc.noaa.gov/data-access/model-data/model-datasets/global-data-assimilation-system-gdas) to estimate likely elevations of condensation, based on humidity,

249 temperature and vertical velocity, and initiates air parcels at these heights. Because the exact
250 time of precipitation for each event was unknown, a series of initiation times was evaluated to
251 represent the most likely periods of the day for convective events typical of spring/summer NN
252 rains. Parcels were first initialized at 12 Mountain Standard Time (MST), and if these failed to
253 produce condensation a new set were initialized at 15 MST, followed by 18 MST, and 9 MST.
254 For each analysis in which condensation occurred, 1000 back trajectories were initialized and
255 tracked for 10 days (240 hours) back in time. Vapor sources were identified as locations where
256 air parcels first intersected the boundary layer (as calculated from the reanalysis data).
257
258 Back trajectory analysis was also performed for July and August 2016 at two sites, Forest Lake,
259 AZ and Smith Lake, NM, which are representative of the western and eastern seasonal
260 precipitation regimes of the NN, respectively. No records of the timing of precipitation events
261 were available for these sites, and back trajectories were initialized at both sites every day of July
262 and August at 12, 3, and 6 MST. For each day and time, 500 air parcels were tracked 10 days
263 (240 hours) back in time.
264

265 **3 Results**

266 3.1 Data Quality and Comparability

267 Summer conditions across the NN are severe, with temperatures often exceeding 35°C and
268 limited precipitation accumulation. Although our precipitation collectors were designed to
269 minimize potential for sample loss to evaporation, which directly affects isotope ratios, we
270 conducted two activities to evaluate our success in this respect. From May to October, 2016, we
271 deployed two identical precipitation collectors, one with and the other without mineral oil, at

each of five monitoring sites distributed across the NN (Beaver Springs, AZ, Bluff, UT, Leupp, AZ, Nageezi, NM, and Rock Springs, NM). Aggregating the data by site or by month, there was no significant difference between the $\delta^{18}O$ values measured for the two methods (Table S1; paired T-test, all $p \geq 0.08$). What differences in the mean isotope ratios did exist were inconsistent, with the oil-free collectors giving slightly higher values, as would be expected to result from evaporative loss of sample water, in most, but not all cases. Likewise, there was no significant difference between the precipitation amounts measured for the two methods with the exception of the average across sites for May ($p = 0.04$), when the no-oil collectors recorded ~20% more precipitation than the collectors containing oil. This suggests that the addition or omission of oil, which has commonly been used to limit evaporation from rainfall collectors (Michelsen et al., 2018), had limited effect on our sample values.

As a second test, we compared data from event-based sampling, in which rainwater was collected as soon as possible (usually within 24 hours) after a precipitation event, with monthly-integrated samples at the two sites where both methods were used in parallel. After filtering for gaps in sampling and missing data, we identified 15 site-months between 2014 and 2017 for which a direct comparison could be made. We calculated precipitation amount-weighted average $\delta^{2}H$ and $\delta^{18}O$ values from the event-based samples. In cases where one or two event samples were missing sample amount information, we substituted the mean amount from other samples from the same site and month and flagged the resulting value of lower quality (4 site-months). Paired t-tests on the $\delta^{18}O$ data, conducted using all records or subsets that removed a single outlier value (July, 2014 at Fort Defiance), both 2014 (no-oil) measurements, or all low-quality data, showed no significant difference between event-based and monthly values (all $p > 0.08$).

295 Across all data, the monthly-integrated values were 1‰ higher, on average, than the event-based
296 values, but this was driven primarily by the single outlier value. The two 2014 samples had the
297 largest differences between monthly- and event-based values (11.0 and 2.5‰), and removing
298 these from the sample-set the monthly-integrated sample values were 0.12‰ higher, on average,
299 than the event-based values. Thus, the results of this test suggest that the long period (1-month)
300 of integration used for the majority of our sampling resulted only minor post-precipitation
301 isotope effects (if any), and that most of our measured values should be representative of
302 unmodified precipitation to within a few tenths of a per mil. Although the sample numbers were
303 small, this test, in contrast to the paired collector test describe above, suggests that the oil-free
304 collectors used in 2014 may have allowed enough evaporative sample loss to substantially
305 modify the isotopic values. Based on both lines of evidence, we retain the 2014 values in our
306 analysis, but interpret them with caution in cases where post-collection evaporative effects might
307 influence our interpretations.
308

309 3.2 Precipitation Isotope Data

310 Precipitation samples exhibit a wide range of values among sites and sampling periods (Fig. 2A-
311 C). The mean values for monsoon season samples (-41.6 and -5.7‰ for δ^2H and $\delta^{18}O$,
312 respectively) are highest, followed by those of pre-monsoon (-61.9 and -8.0‰) and post-
313 monsoon (-66.7 and -9.5‰), respectively. Within each season, values are widely variable. Pre-
314 monsoon precipitation values are most widely dispersed (1σ = 35.5 and 5.9‰), whereas
315 monsoon season (21.6 and 3.6‰) and post-monsoon (21.7 and 3.2‰) variabilities are similar
316 and lower. For each season, a large proportion of samples have values that plot near the global
317 meteoric water line (GMWL: $\delta^2H = 8 \times \delta^{18}O + 10$), which is characteristic of most precipitation

318 that has not experienced partial evaporation following condensation (Craig, 1961; Dansgaard,
319 1964). A substantial fraction of samples, however, particularly for the pre-monsoon and
320 monsoon periods, plot well below the GMWL, as expected for samples that have experienced
321 evaporation. Such samples are present in the data for all years, but are more common in some
322 years and seasons (e.g., 2014 monsoon and post-monsoon, 2016 pre-monsoon, 2017 for all
323 periods) than in others. As discussed in the previous section, we think it is unlikely that most
324 samples experienced substantial evaporation after collection. In hot and dry conditions, such as
325 those that characterize the NN throughout the spring-fall period, sub-cloud evaporation from
326 falling raindrops is a common phenomenon, and is reflected in the isotopic composition of
327 ground-collected rainfall (Gat, 1996; Kong et al., 2013; Salamalikis et al., 2016).
328
329 We used the iSW_E framework to estimate the pre-evaporation composition of each sample (Fig.
330 3A-C). The mean values for evaporation-corrected rainfall samples are substantially lower than
331 the uncorrected values for all seasons (monsoon: -54.9 and -8.4‰; post-monsoon: -76.6 and -
332 11.5‰; pre-monsoon: -78.1 and -11.3‰), and following correction the mean pre- and post-
333 monsoon values are similar but remain distinct from the monsoon distribution. The convergence
334 of the pre- and post-monsoon values reflects the greater degree of evaporation characteristic of
335 the pre-monsoon samples, as shown by the iSW_E evaporation index (mean = 3.3, 2.7, and 2.0‰
336 for pre-monsoon, monsoon, and post-monsoon samples, respectively).
337
338 Navajo Nation hydroclimate varied substantially across the four study years, with 2015 being
339 atypically wet throughout all seasons and 2014 featuring an atypically dry pre-monsoon period
340 (Fig. 4). Despite this, the average monsoon-season precipitation isotope ratios were similar for

all years. Individual year average pre- and post-monsoon values, both measured and evaporation-corrected, were much more variable than the monsoon-season values. Monsoon-season values were higher than pre- or post-monsoon for all years except 2016, when the pre-monsoon value was slightly higher than the monsoon-season average. Following evaporation correction, however, the 2016 pre-monsoon value was ~2‰ lower than the monsoon value, suggesting that the inversion of the pattern during that year reflected high rates of sub-cloud evaporation for the pre-monsoon samples. Relationships between individual-year seasonal-average precipitation amounts and isotope values were relatively weak. Prior to evaporation correction, monsoon period values were weakly, negatively correlated with precipitation amounts, with the lowest average value occurring during 2015. The post-monsoon values were weakly positively correlated with seasonal precipitation amounts (with or without evaporation-correction).

Across all years and samples, precipitation isotope ratios were weakly but significantly correlated with precipitation amount (as measured at the isotope sample collector) only for the pre-monsoon period and for all periods combined (Table 1). In both cases, H and O isotope values decreased with increasing precipitation amount, analogous to the "amount effect" that has long been observed at many tropical and subtropical monitoring sites (Dansgaard, 1964; Rozanski et al., 1993). For all sampling periods, however, the iSW_E evaporation index was significantly correlated with precipitation amount, indicating that the degree of post-condensation evaporative water loss increases during drier sampling periods (Table 1). The magnitude of this effect fully accounts for the observed isotope vs amount correlation for the combined (all periods) dataset, and explains approximately half of the observed correlation for the pre-monsoon data.

364

365 Limited spatial structure was observed in the stable isotope data, regardless of season. Monthly
366 average values (across all 4 study years) for stations within each of the five seasonal
367 hydroclimate cluster groups defined by Tulley-Cordova et al. (2018) exhibited similar patterns
368 across the April-October period, and both patterns and values were very consistent across regions
369 following evaporation correction (Fig. 5). Substantial differences that were observed between
370 some regions for some months (e.g., April, June, and July) were largely attributable to
371 differences in post-condensation evaporative effects, as reflected by the iSW_E evaporation index
372 (Fig. 5C). The data, in particular the evaporation-corrected values, did show some subtle patterns
373 that may reflect hydroclimatic influences. For example, the highest evaporation-corrected
374 precipitation isotope ratios were observed in August for all site groups except the 'East' group,
375 where values peaked in July and dropped by 1.8‰ in August. This difference corresponds with a
376 difference in the timing of peak monsoon precipitation among regions, with precipitation
377 peaking in August at sites in all groups except the East, and in July at the eastern sites (Tulley–
378 Cordova et al., 2018).

379

380 Precipitation isotope ratios were weakly but significantly correlated with site elevation for all
381 periods except the pre-monsoon (Table 2). The same was true of the iSW_E evaporation index.
382 The strongest correlations were observed for the post-monsoon period, wherein site elevation
383 explained up to 14% of the precipitation isotope variance (for $\delta^{18}O$). The slope of the isotope-
384 elevation relationship for this period (-4.1‰/km for $\delta^{18}O$) was relatively high compared with
385 other regions, globally (Poage & Chamberlain, 2001). A substantial fraction of the effect,
386 however, can be attributed to post-condensation evaporation, which decreases with increasing

387 site elevation by 2.1‰/km.

388

389 3.3 Back trajectory analysis

390 Of the 68 events sampled at Rock Springs and 60 events sampled at Fort Defiance between May
391 and October, 2015-2017, back trajectories were successfully initiated for 60 and 54 events,
392 respectively (Fig. 6). Premonsoon and monsoon vapor source regions differed. Premonsoon
393 vapor sources tended to indicate land or Pacific origin vapor, typically traveling from the west
394 into the region, whereas monsoon season vapor tended to indicate dominantly land-sourced
395 vapor. Notably, monsoon season vapor included a large footprint over Mexico, as well as a
396 smaller GoM source contribution. In a few instances, back trajectories indicate precipitation from
397 large synoptic storm systems, carrying distal Pacific vapor into the region; such events are
398 somewhat more common for the pre-monsoon than the monsoon period.

399

400 July and August trajectories at the Forest and Smith Lake sites suggest similar patterns of
401 moisture origin, including major contributions from land surface recycling and additional input
402 from the Pacific/GoC and GoM (Fig. 7). At the eastern site moisture sourced by strong southerly
403 flow is somewhat reduced in August relative to July, whereas both southwesterly and (to a lesser
404 degree) southeasterly flows continue to be the dominant source in August at Forest Lake
405 (western NN).

406

407 3.4 Water resources

408 Isotope ratios of ground waters cluster near or just below the global meteoric water line and near
409 the lower end of the range of precipitation sample values (Fig. 2D). Water resources sampled at

410 the surface, including streams, springs, lake and reservoir samples, are somewhat more variable
411 in their isotopic compositions, and include many samples that plot well below the GMWL (with
412 relatively low d-excess values). This is particularly true for lake samples, most of which have
413 low d-excess values and cluster along a line in δ^2H-$\delta^{18}O$ space that has a slope of ~5.5, similar to
414 but slightly higher than that estimated for open-water evaporation in this region (Bowen et al.,
415 2018). A small number of spring samples also have low d-excess values, possibly reflecting
416 some amount of evaporative loss between the time of surface discharge and sample collection.
417 The evaporation-corrected source water values for all sample types cluster tightly, and are
418 relatively ^2H- and ^{18}O-depeleted relative to the distributions for precipitation samples (Fig. 3D).
419
420 The iSW_E mixing model analysis suggests that the contribution of NAM precipitation to surface
421 and groundwater resources is small (Fig. 8), consistent with the observation that most samples
422 have relatively low isotopic values. The median contribution of NAM rain is estimated at 8%,
423 9%, 10%, and 16% for groundwater, springs, streams, and lakes, respectively. The somewhat
424 higher estimated contribution of NAM precipitation to lake water may, in part, reflect the greater
425 extent of evaporation for these samples (in that the larger evaporation correction is associated
426 with greater uncertainty in source-water mixing estimates). This result, however, is relatively
427 insensitive to the evaporation model assumptions used in our analysis (e.g., the median value
428 differs by only 2% if a hypothesized evaporation line slope of 5.5 is adopted). The iSW_E
429 evaporation index distributions suggest that evaporative effects on lake-water $\delta^{18}O$ values are
430 ~4x greater than those affecting any of the other water types (Fig. 8B).
431

4 Discussion

4.1 NAM precipitation isotopes

The new and extensive monitoring data collected here document the isotopic characteristics of NN NAM precipitation over space and time. Across the spring to fall season, these data show substantial, systematic temporal variability in precipitation isotopic compositions, but only weakly express correlative relationships with variables such as elevation and precipitation amount commonly observed at other sites. The relatively weak relationship with precipitation amount is perhaps unsurprising, as the study area lies outside of the low-latitude zone throughout which this mode of correlation is strongest (Bowen, 2008). Elevation effects, however, are widely observed in other regional precipitation studies (Poage & Chamberlain, 2001). We suggest that their weak expression here may in part relate to the localized and convective nature of NAM and shoulder-season precipitation, which may reduce the isotopic effect of rainout typically associated with orographic lifting of synoptic systems. The suggestion that orographic isotope effects are weaker for convective (vs. synoptic) systems is supported by the observation that isotope-elevation correlations in the NN data are strongest for the post-monsoon and full-year datasets, which encompass periods during which synoptic scale systems are likely to contribute substantially to precipitation.

Where precipitation amount and elevation correlations do exist in the NN data, our analysis suggests they are often associated with variation in post-condensation evaporation. Sub-cloud evaporation of falling raindrops is common in a wide range of meteorological settings characterized by low near-surface humidity and/or rainfall rates (Rindsberger et al., 1990; Worden et al., 2007; Mix et al., 2019) and its isotopic expression has previously been documented with the NAM (Quezadas et al., 2021). Our data suggest that the level of

456 evaporation-drive enrichment of heavy isotopes in rainfall may vary systematically across
457 seasons and sites. The strongest evaporation index values estimated here occurred during the dry
458 and hot pre-monsoon season, producing measured rain sample values that approached or
459 exceeded those of the monsoon season despite estimated pre-evaporation condensate values that
460 were 4-8‰ lower than for NAM rains. The full extent of the observed isotope-precipitation
461 amount correlations observed here, and half or more of the elevation effects, can be attributed to
462 differences in evaporation among sites and sample periods (Tables 1 and 2). This highlights the
463 potential for systematic variation in post-condensation effects to produce structured spatial
464 and/or temporal variation in isotope ratios of precipitation arriving at the land surface.
465
466 The most distinctive feature of NN precipitation isotope data from the intensively sampled
467 spring-to-fall period is the pronounced maximum during the peak monsoon months of July and
468 August (Fig. 5). Across the study region, monthly mean $\delta^{18}O$ values for this period are typically
469 between -3 and -6‰. Outside of the peak monsoon season, values in this range are rare, and are
470 generally associated with a high degree of post-condensation evaporation, implying that the
471 isotope values for atmospheric moisture transported to the NN during the peak of the NAM are
472 substantially higher than those during the immediate pre-and post-monsoon periods (Fig. 5B).
473 This pattern differs from that observed for precipitation in Tucson, AZ, some 400 km to the
474 south, where ground-collected precipitation $\delta^{18}O$ values, and even more so evaporation-corrected
475 values, remain relatively stable from April or May through October (Fig. 5). Moreover,
476 precipitation isotope values for the NN and Tucson converge and are nearly identical during the
477 peak monsoon months, despite the large difference in proximity to marine moisture sources for
478 these two areas.

479

480 We suggest that the convergence between NN and Tucson precipitation isotope ratios during the
481 peak NAM reflects substantial sub-cloud and land-surface moisture recycling during the
482 propagation of NAM moisture to the Four Corners Region. Recycling returns moisture to the
483 atmosphere with similar, or higher, isotope ratios than those of the precipitation source,
484 diminishing or eliminating coast-to-continent gradients otherwise typically associated with the
485 progressive rainout of vapor from air masses (Gat & Matsui, 1991; Ingraham & Taylor, 1991;
486 Winnick et al., 2014). Land-surface recycling has previously been identified as a prominent
487 mechanism for the propagation of NAM rains to the continental interior (Dominguez & Kumar,
488 2008), and will be discussed further below. Sub-cloud evaporation of falling droplets, discussed
489 above, is a second mechanism which can reduce isotope effects associated with rainout (Worden
490 et al., 2007), and is clearly implicated within the dataset examined here based on the relatively
491 large evaporation effects estimated from both NN and Tucson precipitation samples (though
492 perhaps of reduced significance during the peak NAM months; Fig. 5C). We suggest that as the
493 monsoonal circulation intensifies, the penetration of moisture to the northern reaches of the
494 NAM is accompanied and facilitated by high rates of sub-cloud and land-surface recycling,
495 which also drives a large increase in the $\delta^{18}O$ values of NN precipitation and a collapse of the
496 isotopic gradient between this region and upwind, source-proximal areas. Further to the north, at
497 Cedar City, UT, isotope ratios of summer rainfall associated with NAM-like circulation ($\delta^{18}O \approx$ -
498 8.5‰) are higher than those associated with other circulation trajectories but somewhat lower
499 than NN NAM season values (Friedman et al., 2002). This area lies outside of the core NAM
500 region, and the net rainout from the relatively rare and weak monsoon-associated events arriving
501 at Cedar City is likely greater, with a larger isotopic impact, than at the NN.

An additional potential source of variation in NAM-season precipitation isotope ratios is differences or changes in the balance of water arriving from different moisture sources (Hu & Dominguez, 2015). The increase in precipitation isotope values characterizing the onset of the monsoon season is associated with a shift from mid-latitude oceanic and continental moisture sources to GoM and Pacific/GoC sources and subtropical continental sources associated with circulation off of these oceanic regions (Fig. 6). Onset of high-δ^2H and $\delta^{18}O$ moisture transport from these warm oceanic sources, then, combined with strong recycling from upwind continental regions, likely drives the seasonal isotopic maximum associated with the NAM. Trajectory analysis within the monsoon season suggests that moisture transport from the southeast, including GoM sources, declines first (in August) in the eastern NN (Fig. 7), coincident with the earlier weakening of NAM rains in that region than across the rest of the NN (Tulley−Cordova et al., 2018). Weaker August precipitation in the eastern NN appears to be sourced primarily from the southwest/GoC, with secondary additions from the continental interior, and the lower isotope ratios characteristic of these sources may explain the early decline in evaporation-corrected isotope values in this region during August, the month when maximum values are reached elsewhere across the NN (Fig. 5).

Although proxy data recording the isotopic composition of ancient precipitation have been widely used to reconstruct continental paleoclimate, growing recognition that controls on variation in precipitation isotope ratios are diverse and variable has required re-thinking traditional approaches to this work (Schmidt et al., 2007; Liu et al., 2010; Chamberlain et al., 2014; Putman et al., 2021). Our characterization of NAM and shoulder-season precipitation from

525 the Four Corners suggests that controls on isotope ratios in this region are diverse and likely
526 include changes in moisture source, land surface recycling in upwind regions, and local sub-
527 cloud evaporation. Although our monitoring spanned only four years, substantial differences in
528 hydroclimate particularly within the pre- and post-monsoon seasons, occurred within that
529 window of time. In general, the variability in isotope values between monitoring sites in a given
530 year greatly exceeded the variability in mean NN values across years (Fig. 4), suggesting that
531 extraction of paleoclimate records from precipitation isotope proxy data in this region may be
532 challenging. A possible exception is the inverse correlation between precipitation amounts and
533 isotope ratios, driven by differences in sub-cloud evaporation, which is strongly expressed in the
534 pre-monsoon season (Fig. 4, Table 1). Although it is unlikely that most proxy records would
535 directly reflect isotope ratios of water from this season, the pattern observed here may reflect a
536 more general mechanism by which variation in warm season precipitation intensity is expressed
537 in rainfall isotope ratios and could be reconstructed from proxy data.
538

539 4.2 Fate of NAM water

540 Another common application of precipitation isotope data is in quantifying the contribution of
541 different precipitation sources to plants, animals, or water resources. Here, we investigated the
542 contribution of NAM and post-monsoon (winter) season precipitation to a range of water
543 resources that are essential to the people and ecosystems of the NN. We found that, although the
544 NAM contributes approximately 50% of total annual precipitation across most of the study area,
545 its contribution to surface and groundwater resources was minimal, constituting only ~10% of
546 total inputs, on average (Fig. 8). This result is consistent with isotope-based estimates from
547 springs in the Grand Canyon region of Northern Arizona (Solder & Beisner, 2020), also near the

548 northern margin of the NAM west of our study area. A small number of ephemeral stream
549 samples are exceptions to this pattern, likely reflecting direct runoff of NAM rainfall, and
550 estimated contributions from highly-evaporated lakes and reservoirs are relatively uncertain and
551 allow for somewhat higher NAM contributions.
552
553 Despite accounting for multiple sources of uncertainty, the isotope mass balance estimates
554 calculated here are admittedly approximate. The limitations of our approach include relatively
555 sparse sampling of cool-season precipitation and the potential that recharge includes a substantial
556 fraction of high-elevation or ancient precipitation that is not adequately represented in the
557 isotopic endmembers used here. Nonetheless, our measured values for a range of water types are
558 uniformly much lower than those of NAM precipitation (Fig. 2). Even if some water resource
559 samples were partially derived from another (e.g., high-elevation winter or paleowater) source
560 with substantially lower isotope ratios than the winter source measured here, a substantial
561 contribution from NAM rainfall seems unlikely. Accounting for a 50:50 NAM:winter mixture in
562 a typical surface water sample with $\delta^{18}O$ = -13‰ (and assuming the NAM endmember described
563 in our Methods) would require a mean winter season precipitation value of -20.3‰. Using a
564 typical North American isotopic lapse rate of 2.8‰/km (Poage & Chamberlain, 2001; Dutton et
565 al., 2005), this would imply an implausible mean recharge elevation 3 km higher than our
566 monitoring site (itself at 2007 m).
567
568 Our evidence for a limited contribution of NAM rainfall to surface and subsurface water
569 resources on the NN is perhaps not surprising, and does not imply that these rains are
570 hydrologically unimportant. Previous isotopic work has demonstrated substantial uptake and

571 transpiration of monsoon rainfall by many plant species in this region (Williams & Ehleringer,
572 2000; Williams et al., 2005; English et al., 2007). Moreover, our rainfall data discussed above
573 provides evidence for rainfall re-evaporation and for a large fraction of regional summer rainfall
574 being returned to the atmosphere as evapotranspiration (inferred from weak gradients in
575 precipitation isotope ratios across the NAM region). Together, these lines of evidence point to
576 land-atmosphere flux as the primary fate for NAM precipitation in this region, consistent with,
577 and supported by, the lack of evidence for significant monsoon recharge of surface or subsurface
578 water resources.
579

580 **5 Conclusions**

581 Our new data document spatial, temporal, and water resource-related patterns of water H and O
582 stable isotope values across the sparsely sampled Four Corners region of the southwestern
583 United States. We identify variation in atmospheric water sources and post-condensation
584 evaporation as two primary drivers of warm season (spring through fall) precipitation isotope
585 ratio change, and suggest that a shift to low-latitude vapor sources combined with very strong
586 land-surface recycling in upwind areas combine to produce the prominent isotopic maximum
587 associated with North American Monsoon rainfall. Our analysis suggests that NAM rainfall,
588 though volumetrically significant, contributes minimally to regional ground and surface water
589 resources. Instead, we argue that the primary fate for NAM precipitation is re-evaporation (and
590 transpiration). Groundwaters, lakes, streams, and springs located in this region are thus unlikely
591 to be strongly sensitive to future changes in the North American monsoon, but impacts of
592 monsoon change on plant species that are adapted to use summer rains and on water recycling
593 feedbacks that can sustain and propagate NAM-derived moisture to the continental interior (e.g.,

Dominguez et al., 2009) may be more significant.

Acknowledgments

The authors thank the Navajo Nation Water Management Branch's Water Monitoring and Inventory Section, especially Irving Brady, Jerome Bekis, Linda Lee, and Carlee McClellan, Navajo Tribal Utility Authority, particularly Raquel Whitehorse, Navajo citizen scientists, and Tulley and Cordova families who assisted with stable isotopic sample collections. This research has been supported by grant FP-917808 from the U.S. Environmental Protection Agency's Science to Achieve Results (STAR) Program, the Navajo Nation, the Intertribal Timber Council and United States Forest Service's Native American Natural Resources Research Scholarship, the University of Utah's Global Change and Sustainability Center's Research Grant, and US National Science Foundation Grant DEB-1802880. Any opinions, findings, conclusions, or recommendations expressed in this material are those of the authors and do not necessarily reflect the views of the funding agencies. The new water isotope data analyzed in this study are deposited in and were obtained from the Waterisotopes Database (https://waterisotopesDB.org, query: Project = '00066') and all isotope and precipitation data, data processing scripts, and code used to generate figures 2-5 and 8 are archived with Zenodo (https://doi.org/10.5281/zenodo.4628328).

612 **References**

613 Adams, D. K., & Comrie, A. C. (1997). The north American monsoon. *Bulletin of the American*
614 *Meteorological Society, 78*(10), 2197-2214.
615 Aggett, G., Frisbee, M., Harding, B., Miller, G. H., & Weil, P. (2011). *Hydromet Network*
616 *Optimization for the Navajo Nation's Department of Water Resources Water*
617 *Management Branch*. Retrieved from
618 Bennett, T., Maynard, N. G., Cochran, P., Gough, R., Lynn, K., Maldonado, J., . . . Cozzetto, K.
619 (2017). Ch. 12: Indigenous peoples, lands, and resources. In J. Melillo, T. Richmond, &
620 G. Yohe (Eds.), *Climate Change Impacts in the United States: The Third National*
621 *Climate Assessment* (pp. 297-317): U.S. Global Change Research Program.
622 Bhattacharya, T., Tierney, J. E., Addison, J. A., & Murray, J. W. (2018). Ice-sheet modulation of
623 deglacial North American monsoon intensification. *Nature Geoscience, 11*(11), 848-852.
624 Bosilovich, M. G. (2003). Numerical simulation of the large-scale North American monsoon
625 water sources. *108*(D16). doi:10.1029/2002jd003095
626 Bowen, G. J. (2008). Spatial analysis of the intra-annual variation of precipitation isotope ratios
627 and its climatological corollaries. *Journal of Geophysical Research, 113, D05113*.
628 doi:10.1029/2007JD009295
629 Bowen, G. J. (2021). SPATIAL-Lab/isoWater: Paria (Version 0.2.1).
630 doi:10.5281/zenodo.4599209
631 Bowen, G. J., Putman, A., Brooks, J. R., Bowling, D. R., Oerter, E. J., & Good, S. P. (2018).
632 Inferring the source of evaporated waters using stable H and O isotopes. *Oecologia, 187*,
633 1025-1039. doi:10.1007/s00442-018-4192-5

634 Carleton, A. M., Carpenter, D. A., & Weser, P. J. (1990). Mechanisms of interannual variability
635 of the southwest United States summer rainfall maximum. *Journal of Climate, 3*(9), 999-
636 1015.
637 Carrillo, C. M., Castro, C. L., Woodhouse, C. A., & Griffin, D. (2016). Low−frequency
638 variability of precipitation in the North American monsoon region as diagnosed through
639 earlywood and latewood tree−ring chronologies in the southwestern US. *International*
640 *Journal of Climatology, 36*(5), 2254-2272.
641 Chamberlain, C. P., Winnick, M. J., Mix, H. T., Chamberlain, S. D., & Maher, K. (2014). The
642 impact of Neogene grassland expansion and aridification on the isotopic composition of
643 continental precipitation. *Global Biogeochemical Cycles*, 2014GB004822.
644 doi:10.1002/2014GB004822
645 Ciancarelli, B., Castro, C. L., Woodhouse, C., Dominguez, F., Chang, H. I., Carrillo, C., &
646 Griffin, D. (2014). Dominant patterns of US warm season precipitation variability in a
647 fine resolution observational record, with focus on the southwest. *International Journal*
648 *of Climatology, 34*(3), 687-707.
649 Cook, E. R., Woodhouse, C. A., Eakin, C. M., Meko, D. M., & Stahle, D. W. (2004). Long-term
650 aridity changes in the western United States. *Science, 306*, 1015-1018.
651 Craig, H. (1961). Isotopic variations in meteoric waters. *Science, 133*, 1702-1703.
652 Crimmins, M. A., Selover, N., Cozzetto, K., & Chief, K. (2013). *Technical Review of the Navajo*
653 *Nation Drought Contingency Plan - Drought Monitoring*. Retrieved from
654 http://www.climas.arizona.edu/publication/report/technical-review-navajo-nation-
655 drought-contingency-plan-drought-monitoring
656 Dansgaard, W. (1964). Stable isotopes in precipitation. *Tellus, 16*(4), 436-468.

657 Dominguez, F., & Kumar, P. (2008). Precipitation recycling variability and ecoclimatological
658 stability-A study using NARR data. Part II: North American Monsoon Region. *Journal of*
659 *Climate, 21*, 5187-5203. doi:10.1175/2008JCLI1760.1
660 Dominguez, F., Villegas, J. C., & Breshears, D. D. (2009). Spatial extent of the North American
661 Monsoon: Increased cross-regional linkages via atmospheric pathways. *Geophysical*
662 *Research Letters, 36, L07401*. doi:10.1029/2008GL037012
663 Dutton, A., Wilkinson, B. H., Welker, J. M., Bowen, G. J., & Lohmann, K. C. (2005). Spatial
664 distribution and seasonal variation in $^{18}O/^{16}O$ of modern precipitation and river water
665 across the conterminous United States. *Hydrological Processes, 19*, 4121-4146.
666 doi:10.1002/hyp.5876
667 Eastoe, C. J., & Dettman, D. L. (2016). Isotope amount effects in hydrologic and climate
668 reconstructions of monsoon climates: Implications of some long-term data sets for
669 precipitation. *Chemical Geology, 430*, 78-89.
670 doi:http://dx.doi.org/10.1016/j.chemgeo.2016.03.022
671 English, N. B., Dettman, D. L., Sandquist, D. R., & Williams, D. G. (2007). Past climate changes
672 and ecophysiological responses recorded in the isotope ratios of saguaro cactus spines.
673 *Oecologia, 154*, 247-258.
674 Friedman, I., Harris, J. M., Smith, G. I., & Johnson, C. A. (2002). Stable isotope composition of
675 waters in the Great Basin, United States 1. Air-mass trajectories. *Journal of Geophysical*
676 *Research, 107*(D19), 4400. doi:10.1029/2001JD000565
677 Garfin, G. M., Ellis, A., Selover, N., Anderson, D. M., Tecle, A., Heinrich, P., . . . Harvey, C.
678 (2007). *Assessment of the Navajo Nation Hydroclimate Network*. Retrieved from https://
679 www.climas.arizona.edu/sites/default/files/pdfnavajo-hydromet-assess-2007.pdf

680 Gat, J. R. (1996). Oxygen and Hydrogen Isotopes in the Hydrologic Cycle. *Annual Review of*
681 *Earth and Planetary Sciences, 24*, 225-262.
682 Gat, J. R., & Matsui, E. (1991). Atmospheric water balance in the Amazon Basin: an isotopic
683 evapotranspiration model. *Journal of Geophysical Research, 96*, 13,179-113,188.
684 Gelman, A., & Rubin, D. B. (1992). Inference from iterative simulation using multiple
685 sequences. *Statistical Science, 7*(4), 457-472.
686 Good, S. P., Mallia, D. V., Lin, J. C., & Bowen, G. J. (2014). Stable Isotope Analysis of
687 Precipitation Samples Obtained via Crowdsourcing Reveals the Spatiotemporal Evolution
688 of Superstorm Sandy. *PLoS ONE, 9*(3), e91117. doi:10.1371/journal.pone.0091117
689 Guiterman, C. H. (2015). *Climatic sensitivities of Navajo forestlands: Use-inspired research to*
690 *guide tribal forest management*. Retrieved from University of Arizona, Tucson, AZ:
691 http://www.climas.arizona.edu/sites/default/files/pdfclimas-fellow-
692 finalreport2014guiterman.pdf
693 Gutzler, D. S. (2000). Covariability of spring snowpack and summer rainfall across the
694 southwest United States. *Journal of Climate, 13*(22), 4018-4027.
695 Hart, R. J., & Fisk, G. G. (2014). *Field Manual for the Collection of Navajo Nation Streamflow-*
696 *Gage Data*: US Department of the Interior, US Geological Survey Open-File Report
697 2013-1107.
698 Hu, H., & Dominguez, F. (2015). Evaluation of Oceanic and Terrestrial sources of moisture for
699 the North American Monsoon using Numerical Models and Precipitation Stable Isotopes.
700 *Journal of Hydrometeorology, 16*, 19-35.

701 Ichiyanagi, K., & Yamanaka, M. D. (2005). Interannual variation of stable isotopes in
702 precipitation at Bangkok in response to El Ñino Southern Oscillation. *Hydrological*
703 *Processes, 19*(17), 3413-3423. doi:10.1002/hyp.5978
704 Ingraham, N. L., & Taylor, B. E. (1991). Light stable isotope systematics of large-scale
705 hydrologic regimes in California and Nevada. *Water Resources Research, 27*(1), 77-90.
706 Kong, Y., Pang, Z., & Froehlich, K. (2013). Quantifying recycled moisture fraction in
707 precipitation of an arid region using deuterium excess. *Tellus B: Chemical and Physical*
708 *Meteorology, 65*(1), 19251. doi:10.3402/tellusb.v65i0.19251
709 Liu, Z., Bowen, G. J., & Welker, J. M. (2010). Atmospheric circulation is reflected in
710 precipitation isotope gradients over the conterminous United States. *Journal of*
711 *Geophysical Research, 115, D22120*. doi:10.1029/2010JD014175
712 Michelsen, N., Van Geldern, R., Roßmann, Y., Bauer, I., Schulz, S., Barth, J. A. C., & Schüth,
713 C. (2018). Comparison of precipitation collectors used in isotope hydrology. *Chemical*
714 *Geology, 488*, 171-179. doi:10.1016/j.chemgeo.2018.04.032
715 Milly, P. C. D., & Dunne, K. A. (2020). Colorado River flow dwindles as warming-driven loss
716 of reflective snow energizes evaporation. *Science, 367*(6483), 1252-1255.
717 doi:10.1126/science.aay9187
718 Mix, H., Reilly, S., Martin, A., & Cornwell, G. (2019). Evaluating the Roles of Rainout and
719 Post-Condensation Processes in a Landfalling Atmospheric River with Stable Isotopes in
720 Precipitation and Water Vapor. *Atmosphere, 10*(2), 86. doi:10.3390/atmos10020086
721 Nania, J., Cozzetto, K., Gillett, N., Druen, S., Tapp, A. M., Eitner, M., . . . Assessment, W. W.
722 (2014). *Considerations for climate change and variability adaptation on the Navajo*

Nation. Retrieved from University of Colorado, Boulder, Colorado: https://wwa.colorado.edu/publications/reports/navajo_report4_9.pdf

Novak, R. M. (2007). *Climate variability and change in the Chuska Mountain area: Impacts, information, and the intersection of western science and traditional knowledge.* (M.S.). University of Arizona, Tucson, Arizona. Retrieved from https://www.geo.arizona.edu/Antevs/Theses/NovakMS2007.pdf

Overpeck, J., & Udall, B. (2010). Dry times ahead. *Science, 328*(5986), 1642-1643.

Plummer, M. (2019). rjags: Bayesian graphical models using MCMC. R package version 4-10. https://CRAN.R-project.org/package=rjags. Retrieved from https://CRAN.R-project.org/package=rjags

Poage, M. A., & Chamberlain, C. P. (2001). Empirical relationships between elevation and the stable isotope composition of precipitation and surface waters: Considerations for studies of paleoelevation change. *American Journal of Science, 301*(1), 1-15.

Putman, A. L., Bowen, G. J., & Strong, C. (2021). Local and regional modes of hydroclimatic change expressed in modern multidecadal precipitation oxygen isotope trends. *Geophysical Research Letters, 48*(5). doi:10.1029/2020gl092006

Putman, A. L., Feng, X., Posmentier, E. S., Faiia, A. M., & Sonder, L. J. (2017). Testing a Novel Method for Initializing Air Parcel Back Trajectories in Precipitating Clouds Using Reanalysis Data. *Journal of Atmospheric and Oceanic Technology, 34*(11), 2393-2405. doi:10.1175/jtech-d-17-0053.1

Putman, A. L., Feng, X., Sonder, L. J., & Posmentier, E. S. (2017). Annual variation in event-scale precipitation δ^2H at Barrow, AK, reflects vapor source region. *Atmospheric Chemistry and Physics, 17*(7), 4627-4639.

746 Putman, A. L., Fiorella, R. P., Bowen, G. J., & Cai, Z. (2019). A global perspective on local
747 meteoric water lines: Meta−analytic insight into fundamental controls and practical
748 constraints. *Water Resources Research, 55*(8), 6896-6910.
749 Quezadas, J. P., Adams, D., Sánchez Murillo, R., Lagunes, A. J., & Rodríguez Castañeda, J. L.
750 (2021). Isotopic variability ($\delta^{18}O$, $\delta^{2}H$ and d-excess) during rainfall events of the north
751 American monsoon across the Sonora River Basin, Mexico. *Journal of South American*
752 *Earth Sciences, 105*, 102928. doi:10.1016/j.jsames.2020.102928
753 R Core Team. (2020). R: A language and environment for statistical computing. *R Foundation*
754 *for Statistical Computing, Vienna, Austria.* https://www.R-project.org/.
755 Redsteer, M. H., Bemis, K., Chief, K., Gautam, M., Middleton, B. R., Tsosie, R., & Ferguson, D.
756 B. b. (2013). Unique challenges facing southwestern tribes. In *Assessment of climate*
757 *change in the southwest United States* (pp. 385-404): Springer.
758 Redsteer, M. H., Kelley, K. B., Francis, H., & Block, D. (2010). Disaster risk assessment case
759 study: Recent drought on the Navajo nation, southwestern United States. In *2011 global*
760 *assessment report on disaster risk reduction* (pp. 1-19). Geneva, Switzerland: United
761 Nations Office for Disaster Risk Reduction.
762 Rindsberger, M., Jaffe, S., Rahamim, S., & Gat, J. (1990). Patterns of the isotopic composition of
763 precipitation in time and space: data from the Israeli storm water collection program.
764 *Tellus B, 42*(3), 263-271.
765 Rozanski, K., Araguás-Araguás, L., & Gonfiantini, R. (1993). Isotopic patterns in modern global
766 precipitation. In *Climate Change in Continental Isotopic Records* (Vol. 78, pp. 1-36).
767 Washington, DC: AGU.

768 Salamalikis, V., Argiriou, A. A., & Dotsika, E. (2016). Isotopic modeling of the sub-cloud
769 evaporation effect in precipitation. *Science of The Total Environment, 544*, 1059-1072.
770 doi:10.1016/j.scitotenv.2015.11.072
771 Schmidt, G. A., LeGrande, A. N., & Hoffmann, G. (2007). Water isotope expressions of intrinsic
772 and forced variability in a coupled ocean-atmosphere model. *Journal of Geophysical*
773 *Research, 112, D10103*. doi:10.1029/2006JD007781
774 Schmitz, J. T., & Mullen, S. L. (1996). Water vapor transport associated with the summertime
775 North American monsoon as depicted by ECMWF analyses. *Journal of Climate, 9*(7),
776 1621-1634.
777 Seager, R., Ting, M. F., Held, I., Kushnir, Y., Lu, J., Vecchi, G., . . . Naik, N. (2007). Model
778 projections of an imminent transition to a more arid climate in southwestern North
779 America. *Science, 316*(5828), 1181-1184. Retrieved from <Go to
780 ISI>://000246724300040
781 Sodemann, H., Masson-Delmotte, V., Schwierz, C., Vinther, B. M., & Wernli, H. (2008).
782 Interannual variability of Greenland winter precipitation sources: 2. Effects of North
783 Atlantic Oscillation variability on stable isotopes in precipitation. *Journal of Geophysical*
784 *Research: Atmospheres, 113*(D12). doi:doi:10.1029/2007JD009416
785 Solder, J. E., & Beisner, K. R. (2020). Critical evaluation of stable isotope mixing end-members
786 for estimating groundwater recharge sources: Case study from the South Rim of the
787 Grand Canyon, Arizona, USA. *Hydrogeology Journal, 28*, 1575-1591.
788 doi:10.1007/s10040-020-02194-y

789 Strong, M., Sharp, Z. D., & Gutzler, D. S. (2007). Diagnosing moisture transport using D/H
790 ratios of water vapor. *Geophysical Research Letters, 34, L03404*, 1-5.
791 doi:10.1029/2006GL028307
792 Su, Y.-S., & Yajima, M. (2020). R2jags: Using R to Run 'JAGS'. R package version 0.6-1.
793 https://CRAN.R-project.org/package=R2jags.
794 Szejner, P., Wright, W. E., Babst, F., Belmecheri, S., Trouet, V., Leavitt, S. W., . . . Monson, R.
795 K. (2016). Latitudinal gradients in tree ring stable carbon and oxygen isotopes reveal
796 differential climate influences of the North American Monsoon System. *Journal of*
797 *Geophysical Research: Biogeosciences, 121*(7), 1978-1991.
798 Treble, P. C., Chappell, J., Gagan, M. K., McKeegan, K. D., & Harrison, T. M. (2005). In situ
799 measurement of seasonal $d^{18}O$ variations and analysis of isotopic trends in a modern
800 speleothem from southwest Australia. *Earth & Planetary Science Letters, 233*, 17-32.
801 doi:doi:10.1016/j.epsl.2005.02.013
802 Tsinnajinnie, L. M., Gutzler, D. S., & John, J. (2018). Navajo Nation Snowpack Variability from
803 1985-2014 and Implications for Water Resources Management. *Journal of Contemporary*
804 *Water Research & Education, 163*(1), 124-138. doi:10.1111/j.1936-704x.2018.03274.x
805 Tulley−Cordova, C. L., Strong, C., Brady, I. P., Bekis, J., & Bowen, G. J. (2018). Navajo Nation,
806 USA, Precipitation Variability from 2002 to 2015. *Journal of Contemporary Water*
807 *Research and Education, 163*(1), 109-123.
808 Wildcat, D. R. (2013). Introduction: climate change and indigenous peoples of the USA.
809 *Climatic Change, 120*(3), 509-515. doi:10.1007/s10584-013-0849-6
810 Williams, D. G., Coltrain, J. B., Lott, M. J., English, N. B., & Ehleringer, J. R. (2005). Oxygen
811 isotopes in cellulose identify source water for archaeological maize in the American

812 Southwest. *Journal of Archaeological Science, 32*(6), 931-939.
813 doi:10.1016/j.jas.2005.01.008
814 Williams, D. G., & Ehleringer, J. R. r. (2000). Intra- and interspecific variation for summer
815 precipitation use in pinyon-juniper woodlands. *Ecological Monographs, 70*(4), 517-537.
816 Winnick, M. J., Chamberlain, C. P., Caves, J. K., & Welker, J. M. (2014). Quantifying the
817 isotopic 'continental effect'. *Earth and Planetary Science Letters, 406*, 123-133.
818 Worden, J., Noone, D., Bowman, K., Beer, R., Eldering, A., Fisher, B., . . . Worden, H. (2007).
819 Importance of rain evaporation and continental convection in the tropical water cycle.
820 *Nature, 445*, 528-532. doi:10.1038/nature05508
821

822 Table 1: Linear regression statistics describing the correlation between precipitation isotope
823 values and precipitation amount (in mm; bold: $p < 0.05$).

Period	δ^2H vs Amount		$\delta^{18}O$ vs Amount		Evaporation vs Amount	
	Slope	R^2	Slope	R^2	Slope	R^2
All	**-0.135**	**0.012**	**-0.042**	**0.048**	**-0.046**	**0.121**
Pre-monsoon	**-1.018**	**0.265**	**-0.172**	**0.262**	**-0.078**	**0.124**
Monsoon	-0.126	0.019	-0.035	0.057	**-0.037**	**0.113**
Post-monsoon	0.158	0.023	-0.017	0.005	**-0.06**	**0.184**

824

825

826 Table 2: Linear regression statistics describing the correlation between precipitation isotope
827 values and site elevation (in km; bold: $p < 0.05$).

Period	δ^2H vs Elevation		$\delta^{18}O$ vs Elevation		Evaporation vs Elevation	
	Slope	R^2	Slope	R^2	Slope	R^2
All	**-9.7**	**0.01**	**-2.1**	**0.018**	**-1.4**	**0.018**
Pre-monsoon	-5.6	0	-1.3	0.001	-0.6	0
Monsoon	**-6.8**	**0.007**	**-1.7**	**0.019**	**-1.6**	**0.031**
Post-monsoon	**-21.4**	**0.08**	**-4.1**	**0.139**	**-2.1**	**0.048**

828

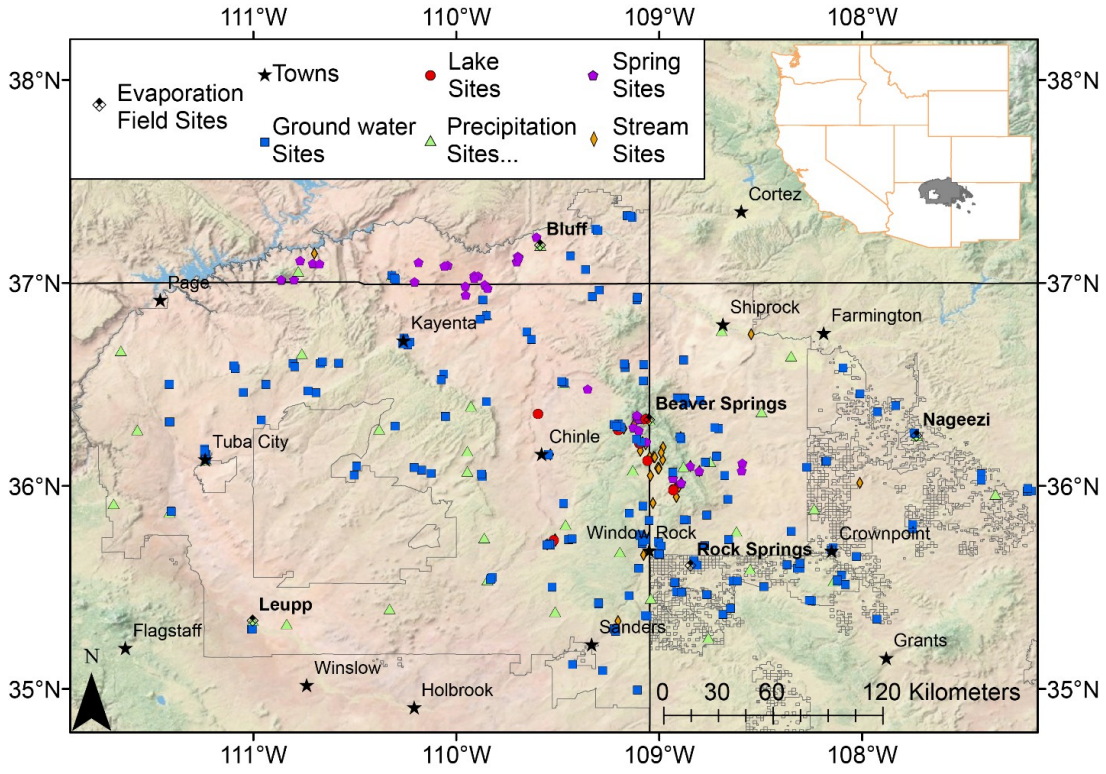

Figure 4. Sampling sites within the boundaries of the Navajo Nation (grey lines). Bold names denote evaporation experiment field sites.

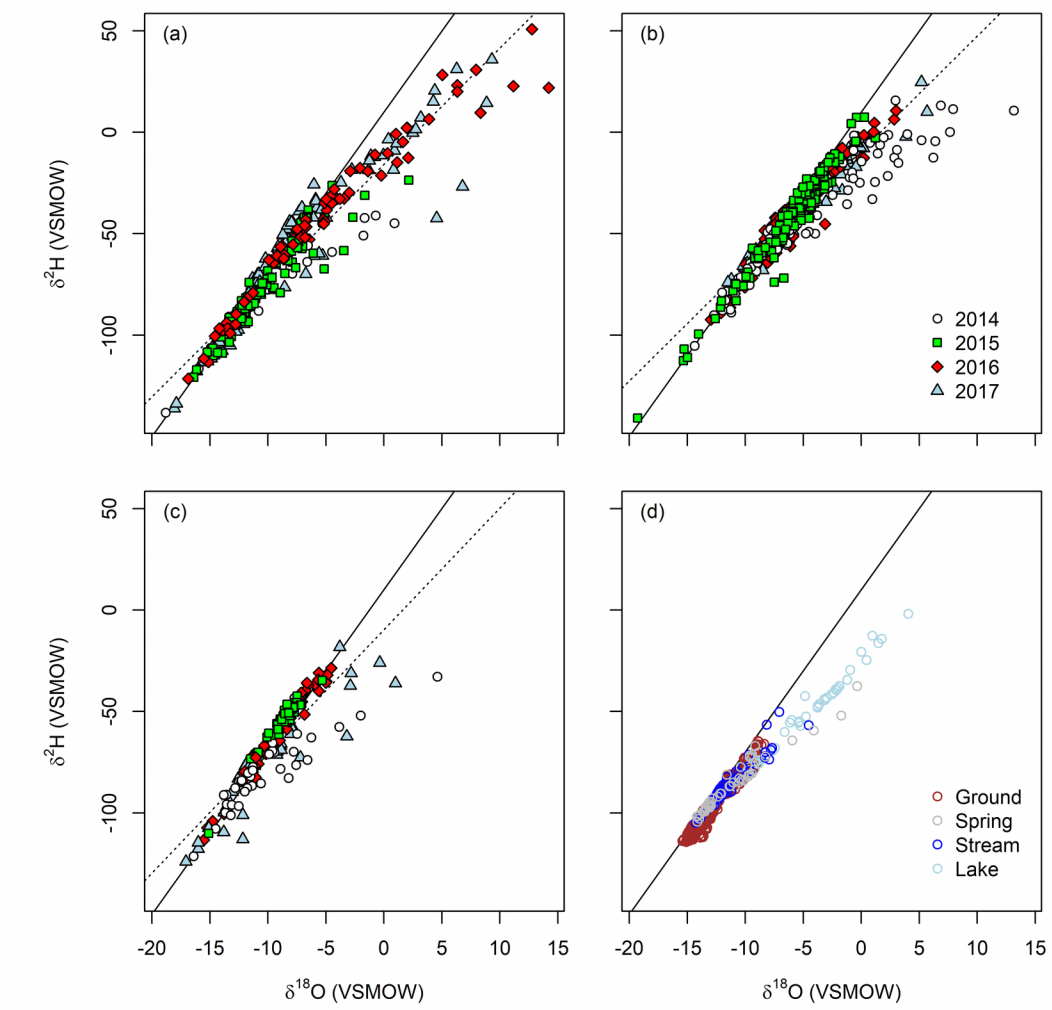

Figure 2: Stable H and O isotope ratios of water samples from the Navajo Nation. Panels show precipitation from (a) pre-monsoon, (b) monsoon, or (c) post-monsoon seasons, and from surface and groundwater samples (d). Dotted lines are regressions through each dataset (a-c), and the solid line in each panel shows the Global Meteoric Water Line.

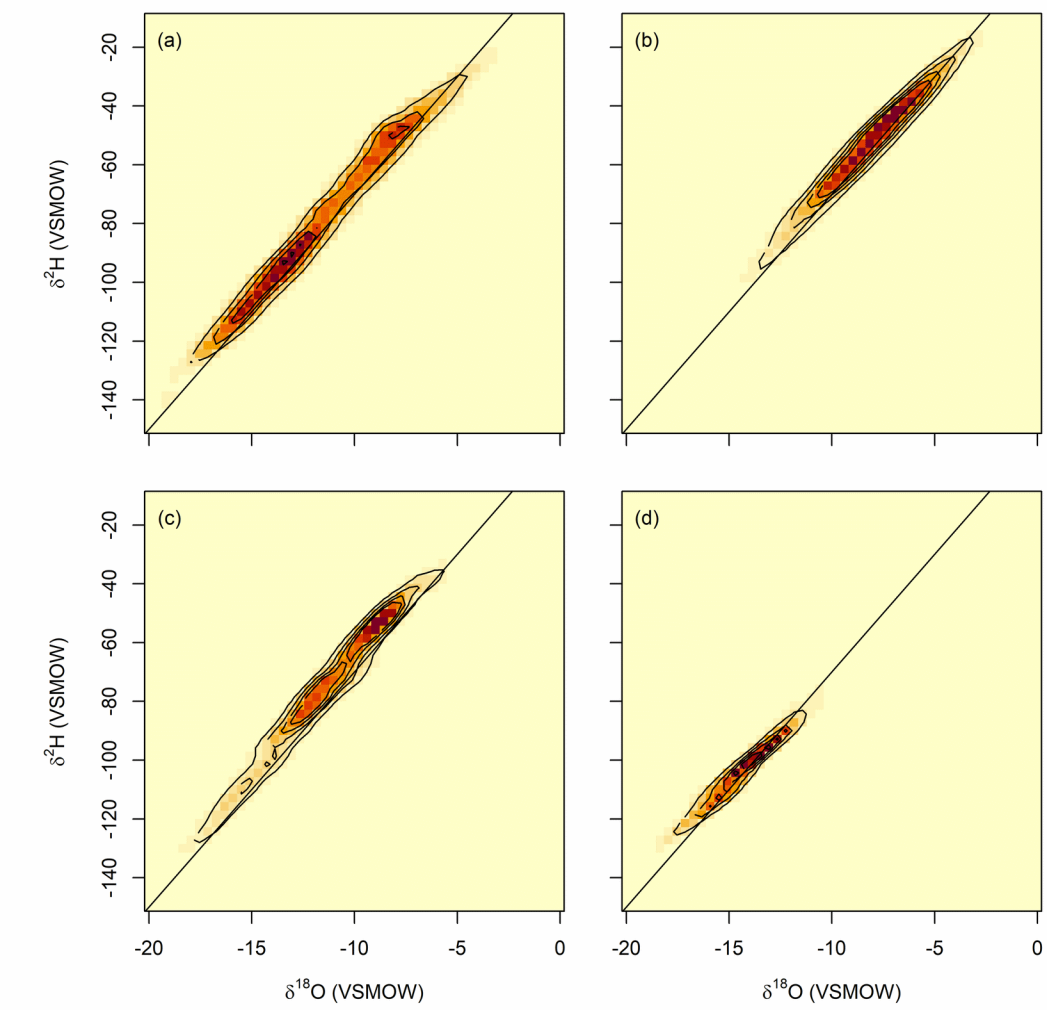

Figure 3: 2-dimensional density plots showing the distribution of water isotope values for Navajo Nation samples following correction for post-condensation evaporation effects. Panels show distributions for (a) pre-monsoon, (b) monsoon, and (c) post-monsoon precipitation and (d) surface and subsurface water resources. Colors are proportional to the density of source water isotope values in the posterior distribution of the iSW_E analysis, and contours separate density values at intervals of 0.2% in A-C and 0.6% in (d). The solid line in each panel shows the Global Meteoric Water Line.

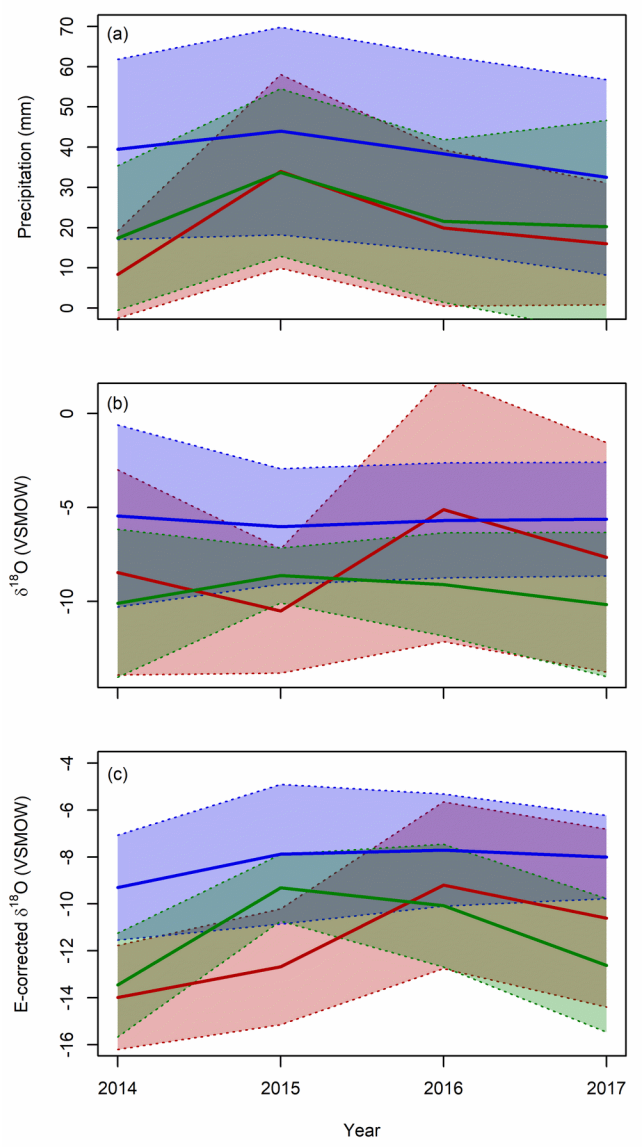

Figure 4: Inter-annual trends in seasonal precipitation and isotope data across the Navajo Nation, showing mean values and 1σ ranges for pre-monsoon (red), monsoon (blue), and post-monsoon (green) months. Panels show precipitation amount (a), measured precipitation $\delta^{18}O$ values (b), and precipitation O-isotope values corrected for post-condensation evaporation effects (c).

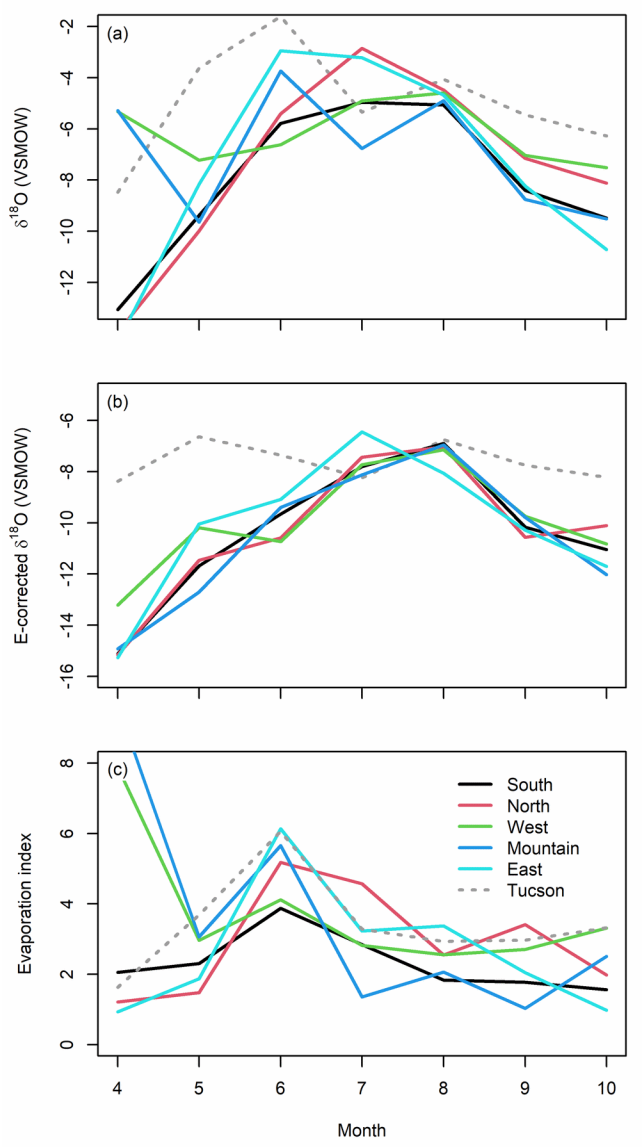

Figure 5: Monthly average precipitation isotope values for monitoring sites within each of five groups having contrasting seasonal precipitation patters (defined by Tulley−Cordova et al., 2018) and at Tucson, AZ (Eastoe & Dettman, 2016). A) Measured oxygen isotope values. B) Oxygen isotope values after correction of evaporation effects using the iSW_E method (see Methods; Bowen et al., 2018). C) The iSW_E oxygen isotope evaporation index (higher index value indicates a larger amount of post-condensation evaporation).

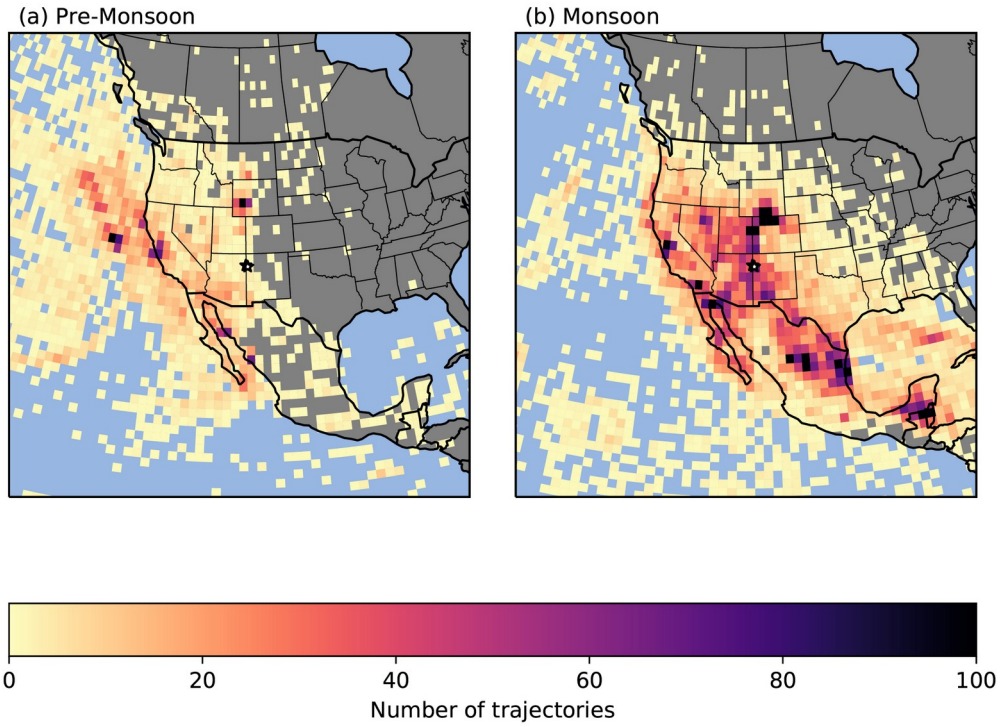

Figure 6. Spatial distribution of the vapor source region by season for combined precipitation events at Rock Springs, NM and Fort Defiance, AZ, with the representative location indicated by star. This figure shows the number of trajectories traced to a vapor source in a particular pixel during the premonsoon season (a) and monsoon season (b).

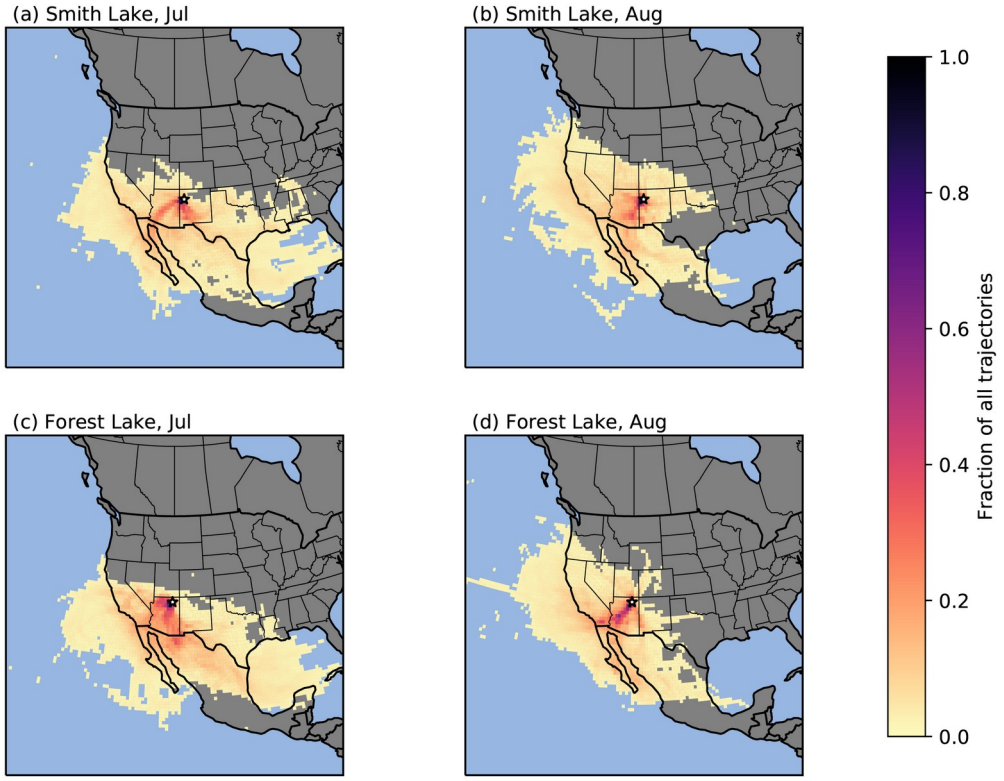

Figure 7. Spatial and temporal evolution of air mass trajectories into the Eastern (Smith Lake, NM, panels a and b) and Western (Forest Lake, AZ, panels c and d) regions of the Navajo Nation as monsoon season develops between the months of July (panels a and c) and August (panels b and d), 2016.

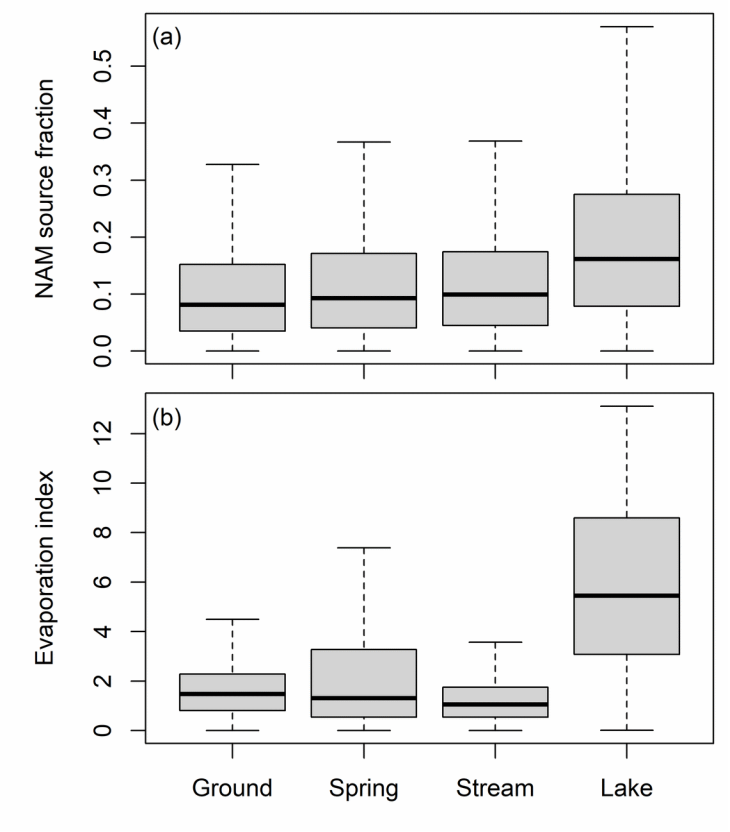

Figure 8: Posterior parameter distributions for water resource mixing model analyses. A) Estimated fractional contribution of NAM rainfall to sampled water resources. B) Oxygen isotope evaporation index distributions for each resource type. Outlier values are omitted.

873